The small GTPases ARL-13 and ARL-3 coordinate intraflagellar transport and ciliogenesis

Yujie Li,[1] Qing Wei,[1] Yuxia Zhang,[1] Kun Ling,[2] and Jinghua Hu[1,2]

[1]Division of Nephrology and Hypertension, Department of Internal Medicine, and [2]Department of Biochemistry and Molecular Biology, Mayo Clinic, Rochester, MN 55905

Intraflagellar transport (IFT) machinery mediates the bidirectional movement of cargos that are required for the assembly and maintenance of cilia. However, little is known about how IFT is regulated in vivo. In this study, we show that the small guanosine triphosphatase (GTPase) adenosine diphosphate ribosylation factor–like protein 13 (ARL-13) encoded by the *Caenorhabditis elegans* homologue of the human Joubert syndrome causal gene *ARL13B*, localizes exclusively to the doublet segment of the cilium. *arl-13* mutants have shortened cilia with various ultrastructural deformities and a disrupted association between IFT subcomplexes A and B. Intriguingly, depletion of ARL-3, another ciliary small GTPase, partially suppresses ciliogenesis defects in *arl-13* mutants by indirectly restoring binding between IFT subcomplexes A and B. Rescue of *arl-13* mutants by ARL-3 depletion is mediated by an HDAC6 deacetylase-dependent pathway. Thus, we propose that two conserved small GTPases, ARL-13 and ARL-3, coordinate to regulate IFT and that perturbing this balance results in cilia deformation.

Introduction

Cilia, which act as motile or sensory devices on the surfaces of most eukaryotic cells, play essential roles in development and postnatal tissue pattern formation. Mounting evidence links defects in cilia biogenesis and/or function to a wide spectrum of human genetic disorders that have been collectively termed ciliopathies (Badano et al., 2006). Joubert syndrome (JS) is an autosomal recessive disorder characterized by abnormalities in the central nervous system and by various commonly shared ciliopathy manifestations such as cystic kidney, blindness, and polydactyly. The functions of all identified JS loci (*NPHP1*, *AHI1*, *CEP290*, *RPGRIP1L*, *TMEM67/MKS3*, *Arl13B*, and *CC2D2A*), as well as most other ciliopathy candidate genes, have been suggested to be cilia and/or basal body related. Nonetheless, the precise roles of these genes remain enigmatic (Pazour and Rosenbaum, 2002; for reviews see Eley et al., 2005; Fliegauf et al., 2007; Parisi, 2009).

Intraflagellar transport (IFT) builds and maintains all cilia and flagella (Rosenbaum and Witman, 2002). In *Caenorhabditis elegans*, the head amphid and tail phasmid sensory organs terminate with channel cilia, which are composed of middle segments containing nine peripheral doublet microtubules and distal segments containing singlet microtubules (Perkins et al., 1986). In *C. elegans*, IFT is regulated by two anterograde motor machineries, the canonical heterotrimeric kinesin-II and homodimeric OSM-3/KIF17, and one retrograde dynein motor (Scholey, 2008). The two kinesin motors cooperate to build the middle doublets, whereas OSM-3 acts alone to extend distal singlets (Ou et al., 2005). Kinesin-II associates with IFT subcomplex A (IFT-A), OSM-3 associates with IFT subcomplex B (IFT-B), and the Bardet–Biedl syndrome (BBS) proteins stabilize the association between IFT-A and IFT-B. In the absence of BBS-7 and BBS-8, IFT-A and IFT-B separate as a result of mechanical competition between the two kinesin motors (Ou et al., 2005). Remarkably, both kinesin-II/KIF3 and OSM-3/KIF17 homologues appear to contribute to IFT and ciliogenesis in vertebrate systems (Marszalek et al., 2000; Lin et al., 2003; Jenkins et al., 2006; Insinna et al., 2008, 2009).

ADP ribosylation factor (Arf)–like proteins (Arls) are enzymatically active small GTPases in the Ras superfamily. The family of mammalian Arf/Arl GTPases includes 29 members, and the roles of most Arf/Arls are poorly understood (for

Correspondence to Jinghua Hu: hu.jinghua@mayo.edu

Abbreviations used in this paper: Arf, ADP ribosylation factor; Arl, Arf-like proteins; BBS, Bardet–Biedl syndrome; DA, dominant active; Dyf, dye-filling defective; IFT, intraflagellar transport; JS, Joubert syndrome; NT, N terminal; PRD, proline-rich domain; TEM, transmission electron microscopy; TZ, transition zone.

The Rockefeller University Press $30.00
J. Cell Biol. Vol. 189 No. 6 1039–1051
www.jcb.org/cgi/doi/10.1083/jcb.200912001

reviews see D'Souza-Schorey and Chavrier, 2006; Gillingham and Munro, 2007). In comparative genomic searches, *Arl3* and *Arl6* were identified as genes that are expressed exclusively in ciliated organisms (Avidor-Reiss et al., 2004; Li et al., 2004). Later, human *Arl6* was identified as a locus causative for BBS syndrome, and its *C. elegans* homologue was found to enter the cilium and undergo IFT (Fan et al., 2004). Meanwhile, ARL-3 was found in the *Chlamydomonas reinhardtii* ciliary proteome (Pazour et al., 2005) and implicated in *Leishmania donovani* flagellum biogenesis (Cuvillier et al., 2000). The $Arl3^{(-/-)}$ mouse dies after birth and exhibits typical ciliopathy manifestations such as cystic kidney and photoreceptor degeneration (Schrick et al., 2006). In addition, mutations in another small GTPase, *Arl13b*, cause typical JS disorder, and the $Arl13b^{(-/-)}$ mouse shows coupled defects in cilia structure and Sonic hedgehog signaling (Caspary et al., 2007; Cantagrel et al., 2008). In *C. elegans*, all three ARLs are ciliary proteins (Fan et al., 2004; Blacque et al., 2005). Nonetheless, little is known about the molecular mechanisms of ARLs in cilia.

In this study, we report that in *C. elegans*, ARL-13 localizes exclusively to the doublet segment of the cilium in a manner dependent on its conserved proline-rich domain (PRD). Depletion of ARL-13 causes a disrupted association between IFT-A and IFT-B subcomplexes and various cilia deformities. Intriguingly, depletion of another small GTPase, ARL-3, can partially rescue ciliogenesis defects in *arl-13* mutants by restoring the binding efficiency between IFT-A and IFT-B. Further analyses demonstrated that this specific rescue effect is the result of an attenuated association between IFT-B and the OSM-3 motor in ARL-3–deficient cilia and depends on the deacetylase HDAC6. Thus, our findings provide novel mechanistic insights into small GTPase-mediated regulation of IFT machinery. Moreover, the functional balance between ARL-13 and ARL-3 appears to be critical for proper assembly and maintenance of the IFT motor complex: perturbing this process compromises IFT integrity and results in general cilia deformations.

Results

arl-13 is expressed exclusively in ciliated cells of *C. elegans*

Previous analyses in zebrafish, mouse, and human suggest a highly conserved role for Arl13B protein family members in cilia (Sun et al., 2004; Caspary et al., 2007; Cantagrel et al., 2008; Duldulao et al., 2009). *arl-13*, the *C. elegans* homologue of the human *Arl13b* gene, is expressed exclusively in ciliated sensory neurons throughout development in both hermaphrodites (Fig. S1, A and C; Fan et al., 2004) and males (not depicted), which indicates a distinct ciliary role for ARL-13.

The subcellular localization of ARL-13 was determined by expressing full-length *arl-13* cDNA fused to GFP from the 1.2-kb native promoter (ARL-13::GFP). We found that ARL-13::GFP localized robustly to amphid and phasmid cilia (Fig. 1 B). Strikingly, GFP-tagged ARL-13 was absent from the distal singlet segment of the cilium and from the rest of the neuron, including the neuronal cell body, dendrite, and axon (Fig. 1 B), which suggests that the ARL-13 protein is efficiently targeted to the cilium and plays a specific role within the middle doublet segment.

Our observations of ARL-13 ciliary localization are identical to previously published data (Blacque et al., 2005).We did not observe detectable IFT movement of ARL-13::GFP along the cilium (Fig. S2 A). Analyses of ARL-13::GFP localization in IFT motor mutant *kap-1*(*ok676*) or *osm-3*(*p802*) worms suggest that ARL-13 ciliary targeting does not require the IFT motor kinesin-II or OSM-3 (Fig. S2 B). Both ARL-13 and human Arl13B have a putative N-terminal (NT) palmitoylation motif (Zhou et al., 2006b). The *C. elegans* ARL-$13^{C12\text{-}15Del}$ protein, in which the C12–15 palmitoylation motif has been deleted, localized to both cilia and the cytosol (Fig. S1 D). Quantitation of fluorescence intensity revealed that only ~30% of the ARL-$13^{C12\text{-}15Del}$ protein localized to cilia compared with ~95% of wild-type ARL-13. This observation suggests that ARL-13 is a ciliary membrane-binding small GTPase.

C-terminal PRD restricts ARL-13 to the doublet segment of the cilium

In contrast to most small GTPases, which are ~20 kD and composed of only a GTPase domain, Arl13B has an atypical long C terminus that contains a coiled-coil helix and a PRD (Fig. 1 A). This unique structural pattern is conserved in all Arl13B protein family members from the green algae *C. reinhardtii* to mammals. In zebrafish, ciliary targeting of Arl13B requires both the N and C termini (Duldulao et al., 2009). To characterize the putative cilia targeting signal sequence of *C. elegans* ARL-13, we generated transgenic animals that express different GFP-tagged ARL-13 truncations. Interestingly, both the ARL-13 NT truncation (which retains the GTPase domain plus the coiled-coiled helix) and the ARL-13 PRD truncation (which possesses only the PRD domain) were targeted to cilia (Fig. 1 C), indicating redundant ciliary targeting signals in the N and C termini of the worm ARL-13 protein. Nonetheless, ARL-13 PRD::GFP showed restricted middle segment localization, whereas ARL-13 NT::GFP was present in both middle and distal segments. This result suggests that the PRD domain is critical for restriction of ARL-13 to the doublet segment. Although full-length ARL-13 protein was completely absent from the cell body, we observed significant GFP signals in the cytoplasmic region for ARL-13 NT::GFP and ARL-13 PRD::GFP (Fig. 1 C), which suggests that both the N and C termini are required for efficient ciliary targeting of ARL-13.

ARL-13 is required for amphid and phasmid ciliogenesis

Two deletion alleles are available for the *arl-13* gene, *gk513* and *tm2322*. The *gk513* allele removes a 1.1-kb DNA fragment, including the promoter and first exon (Fig. 1 A). The *tm2322* allele, an in-frame deletion that removes exons 7–9, encodes a truncated protein with an intact GTPase domain (Fig. 1 A). Both *arl-13*(*gk513*) and *arl-13*(*tm2322*) animals are healthy and show no gross anatomical abnormalities. We used *gk513* as a reference allele. Because of the unique expression pattern of the ARL-13 protein (Fig. 1 B), we focused our experiments on cilia.

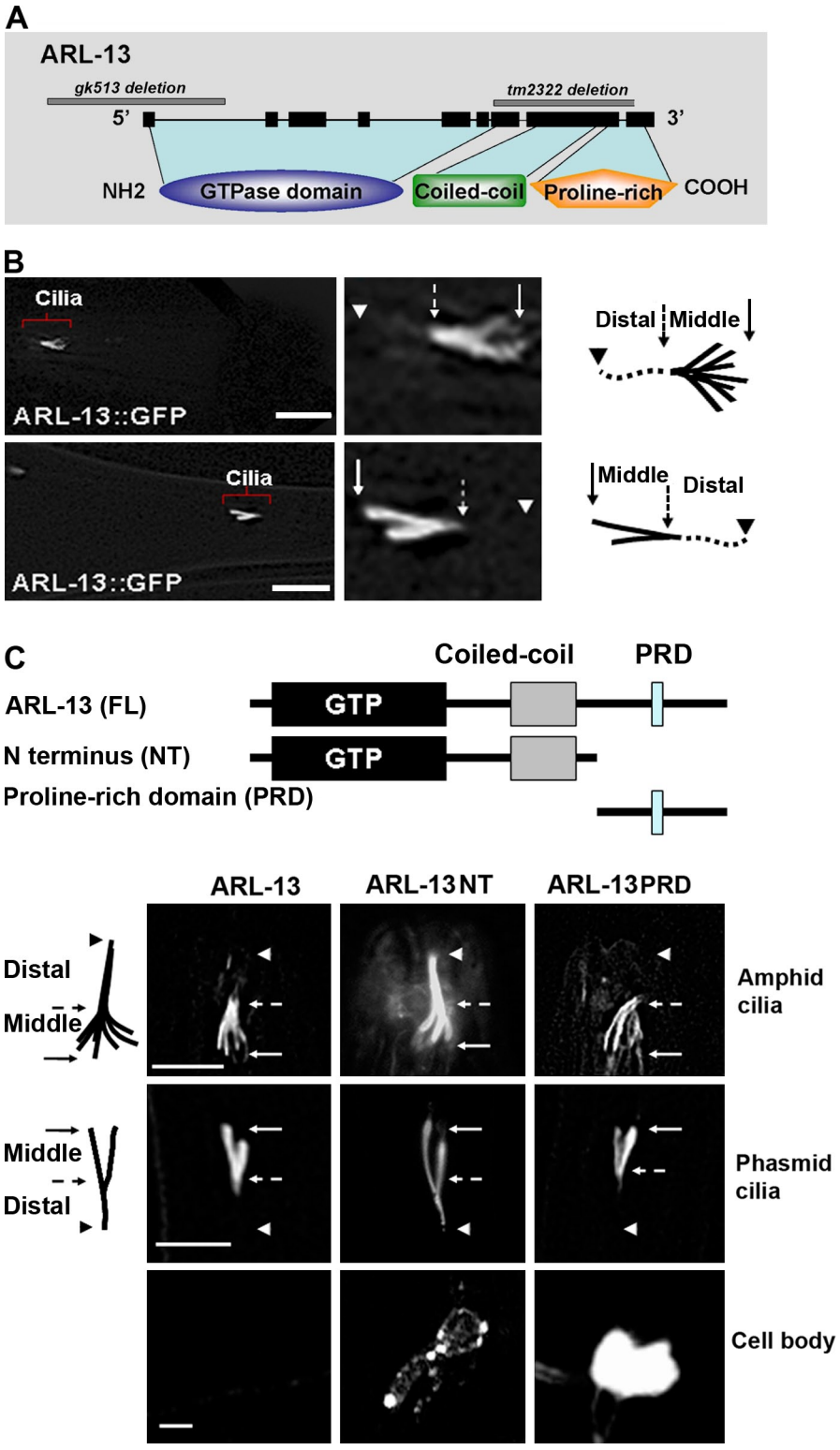

Figure 1. **ARL-13 localizes to middle segments of cilia.** (A) ARL-13 is an atypical GTPase that contains a GTPase domain, a coiled-coil domain, and a proline-rich C terminus. (B) In the adult, ARL-13::GFP was observed only in middle doublet segments. Note that the GFP signal was absent from the distal segment of the cilium as well as from the rest of the neuron, including the neuronal cell body, dendrite, and axon. (C) Transgenic animals that expressed various GFP-tagged ARL-13 truncations were analyzed for cilia targeting. The ARL-13 NT truncation possesses the GTPase and coiled-coil domain (aa 1–250), and the ARL-13 PRD truncation contains the PRD (aa 250–367). ARL-13 NT::GFP was detected in both middle and distal segments, whereas ARL-13 PRD completely mimicked the ciliary localization pattern of full-length (FL) ARL-13. Both truncations showed significant protein retention in cell bodies. Solid arrows indicate TZ, dashed arrows point to the approximate middle to distal segment transition points, and arrowheads mark the distal ends. Bars: (B) 10 µm; (C) 5 µm.

In *C. elegans*, cilia integrity can be assessed by a simple and efficient dye-filling assay. In living worms, amphid and phasmid neurons take up lipophilic fluorescent dye through sensory cilia that are exposed to the outside environment (Hedgecock et al., 1985). Worm mutants with abnormal cilia cannot take up dye and are termed dye-filling defective (Dyf; Perkins et al., 1986). Under the fluorescence dissecting microscope, *arl-13* (*gk513*) amphids showed normal dye uptake, whereas ~40% of phasmids were Dyf (Fig. 2 A). Although no Dyf phenotype was observed in amphids, our transmission electron microscopy (TEM) experiments revealed that some *arl-13*(*gk513*) amphid cilia were malformed (see Fig. 4). The Dyf phenotype of *arl-13* mutants could be fully rescued by introducing an ARL-13::GFP transgene (Fig. 2 A). Furthermore, overexpression of ARL-13

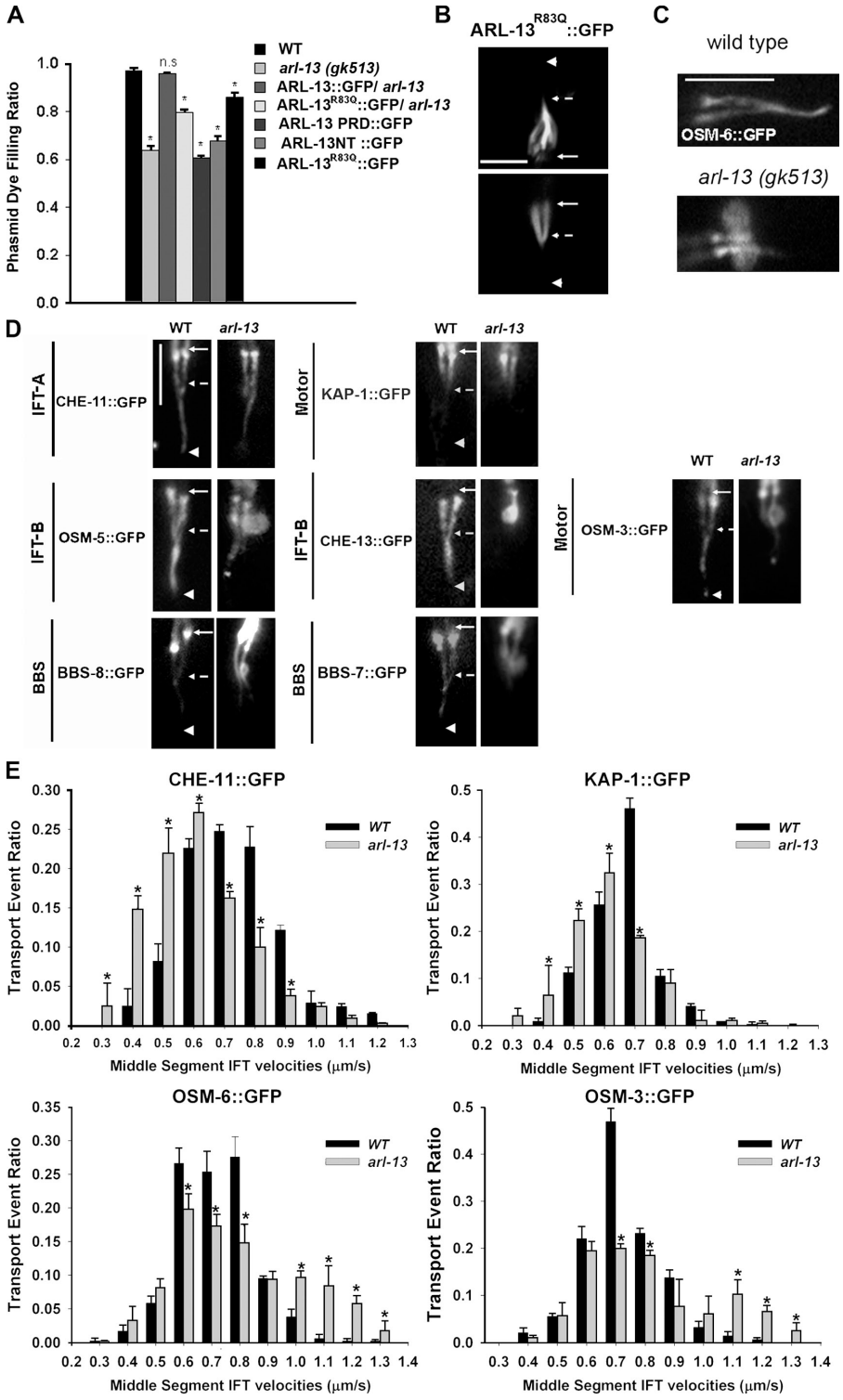

Figure 2. ***arl-13* mutants have deformed cilia and disrupted IFT.** (A) Dye-filling assay was used to examine ciliogenesis. Phasmid cilia of *arl-13* mutants showed a clear Dyf phenotype. Introduction of a copy of wild-type (WT) ARL-13::GFP but not ARL-13^{R83Q}::GFP, which carries a human pathogenic mutation, fully rescued the Dyf phenotype in *arl-13* mutants. Overexpression of ARL-13 NT, ARL-13 PRQ, or ARL-13^{R83Q}::GFP had mild dominant-negative effects on ciliogenesis. At least 100 animals were scored per genotype (~400 individual phasmid cilia were observed). (B) The ciliary localization of ARL-13^{R83Q}::GFP was normal. (C) Phasmid cilia expressing OSM-6::GFP. Note the bulblike accumulations in *arl-13* mutants. (D) Phasmid cilia expressing various ciliary markers. In *arl-13* mutants, the IFT-A component CHE-11::GFP and the kinesin-II motor KAP-1::GFP showed no accumulation along cilia, whereas IFT-B components (CHE-13::GFP and OSM-5::GFP), the IFT-B–associated motor OSM-3, and BBS proteins (BBS-7::GFP and BBS-8::GFP) aggregated in similar bulblike structures. (E) GFP-tagged CHE-11, KAP-1, OSM-6, and OSM-3 were expressed in wild-type and *arl-13* worms, and IFT transport event ratios within middle segments of phasmid cilia were quantified. Note that the curves of the IFT-A component CHE-11 and kinesin-II subunit KAP-1 significantly shifted to the left for *arl-13* mutants compared with wild-type worms, suggesting that significant amounts of IFT-A and the associated kinesin-II move at a slower rate in the mutants. In contrast, a right shift of the curves for the IFT-B component OSM-6 and the OSM-3 motor was observed, indicating that IFT-B and the associated OSM-3 motor tend to move at a faster rate in ARL-13–deficient cilia. In all figures, solid arrows indicate the TZs, dashed arrows point to the approximate middle to distal segment transition points, and arrowheads mark the distal ends. Statistical analysis was performed using a two-tailed paired Student's *t* test. *, $P < 0.01$. Error bars indicate SEM. Bars, 5 μm.

NT::GFP and ARL-13 PRD::GFP both caused Dyf in wild-type animals, which indicates the importance of the GTPase and PRD domains in ARL-13 ciliary function (Fig. 2 A).

We also generated a mutant ARL-13^{R83Q} that resembles the R79Q mutation identified in human JS patients. The human ARL13B^{R79Q} mutant retains half of the GTP-binding efficiency of the wild-type protein (Cantagrel et al., 2008). In *C. elegans*, ARL-13^{R83Q} showed a wild-type ciliary localization pattern (Fig. 2 B). However, as expected, the mutant could only partially rescue the *arl-13*(*gk513*) Dyf phenotype (Fig. 2 A). Overexpression of ARL-13^{R83Q} also caused Dyf in wild-type animals. Collectively, our data suggest a conserved role for the ARL-13 protein and its GTPase activity in ciliogenesis.

arl-13 mutants show various cilia deformations and compromised IFT

We used ciliary markers to examine cilia morphology in *arl-13* mutants. To minimize differences in expression levels of the

markers, we introduced each *gfp* transgene from wild-type strains into *arl-13* mutants by genetic crossing. Expression of OSM-6::GFP, an IFT-B marker, revealed that ~40% phasmid cilia are truncated, and the cilia often show abnormal bulblike structures in the middle segments (Fig. 2 C). This ratio is comparable with the Dyf ratio of *arl-13*(*gk513*) phasmid cilia.

Further analyses revealed that IFT-B proteins (OSM-5, OSM-6, and CHE-13), the IFT-B–associated OSM-3 motor, and IFT regulators (BBS-7 and BBS-8) all accumulated in bulblike structures in middle segments, whereas the IFT-A protein CHE-11 and its associated motor KAP-1 did not exhibit bulblike accumulation along the cilium (Fig. 2 D). All observed bulblike structures were located proximal to the middle to distal transition point (Fig. 2 D, dashed arrows), which might indicate a defective transition of IFT-B subcomplexes (including associated BBS proteins and the OSM-3 motor) from middle segments to distal segments in *arl-13* mutants. In transition zones (TZs; Fig. 2 D, solid arrows), all IFT markers showed similar enrichment in both *arl-13* and wild-type worms.

Next, we examined IFT motility in *arl-13* mutants. In wild-type animals, kinesin-II and OSM-3 cooperate in moving the same IFT particle along the middle segment at 0.7 µm/s. Then, the OSM-3 kinesin alone moves the IFT particle along the distal segment at the faster rate of 1.3 µm/s. Cytoplasmic dynein mediates retrograde movement of the IFT particle along the whole axoneme at a rate of 1.1 µm/s (Signor et al., 1999; Snow et al., 2004; Ou et al., 2005). In *bbs-7* and *bbs-8* mutants, kinesin-II and OSM-3 separate in the middle segment, which results in IFT-A moving with kinesin-II at a slower rate of 0.5 µm/s and IFT-B moving with OSM-3 at a faster rate of 1.3 µm/s (Ou et al., 2005).

In *arl-13* mutants, anterograde IFT movement along distal singlets and retrograde IFT movement occurred at characteristic wild-type rates (Table S1). Because IFT components accumulated abnormally in middle segments, we performed detailed analyses of IFT movement in these regions. The recorded IFT velocities in phasmid cilia were distributed in a normal curve that resembled the previous observation made in amphid cilia (Fig. 2 E; Snow et al., 2004). In *arl-13* mutants, the velocity curves of IFT-A and the IFT-A–associated motor kinesin-II shifted to the left (slower) side, whereas those of IFT-B and the IFT-B–associated motor OSM-3 shifted to the right (faster) side (Fig. 2 E).

To determine the molecular basis of the abnormal IFT movement in *arl-13* mutants, we subtracted the transport event ratio of wild-type animals from that of *arl-13* mutants at each velocity step. Analyses of the distribution curves revealed that in *arl-13* cilia, IFT-A and kinesin-II moved at a rate of ~0.5 µm/s, whereas IFT-B and OSM-3 moved at ~1.3 µm/s (see Fig. 5). For all IFT reporters used in our analyses, fewer IFT particles were found to move at the normal rate of ~0.7 µm/s in *arl-13* mutants than in wild-type animals. These observations suggest that in ARL-13–deficient cilia, the IFT complex tends to dissociate, and the separated subcomplexes are transported by either kinesin-II or OSM-3 alone (see Fig. 7). The dissociation of IFT-A and IFT-B may account for the ciliogenesis defects and accumulation of IFT-B subcomplexes in *arl-13* mutants.

Depletion of ARL-3 partially rescues deformations in ARL-13–deficient cilia

Incomplete dissociation of the IFT complex in *arl-13* cilia indicates the involvement of redundant players in this process. *arl-3* and *arl-6*, the *C. elegans* homologues of human *Arl3* and *Arl6/BBS3*, are promising candidates because they are expressed exclusively in ciliated cells. Similar to ARL-13, ARL-3::GFP does not show detectable movement in cilia (Fig. S2 A), axons, or dendrites (not depicted). In contrast, ARL-6 exhibits typical IFT motility in cilia (Fan et al., 2004). Although ARL-3 was reported to be expressed exclusively in ciliated neurons, with little ciliary localization (Blacque et al., 2005), analysis of our GFP-tagged ARL-3, whose expression was driven by its own 2.5-kb promoter, revealed that a significant amount of ARL-3::GFP localized to cilia (both middle and distal segments; Fig. 3 B). We further analyzed *arl-3*(*tm1703*) mutants, which carry a genomic deletion that encompasses nearly all of the *arl-3* gene (Fig. 3 A). To our surprise, not only were *arl-3*(*tm1703*) animals superficially wild type, they also had no detectable sign of cilia malformation by the dye-filling assay and IFT markers (Fig. 3, C and D).

To address the possibility that *arl-3* negatively regulates ciliogenesis, we generated a transgenic strain that overexpresses ARL-3^{Q72L}, a constitutive GTP-binding (dominant active [DA]) mutant. In accordance with our prediction, DA ARL-3^{Q72L} overexpression caused Dyf in wild-type phasmid cilia (Fig. 3 C). We characterized the genetic interaction between *arl-3* and *arl-13*. As shown in Fig. 3 C, *arl-3; arl-13* double mutants showed less phasmid Dyf, suggesting that depletion of ARL-3 can partly rescue cilia deformations in ARL-13–deficient cilia. This result confirms that ARL-3 negatively regulates ciliogenesis. Consistently, overexpression of DA ARL-3 in *arl-13* had an additive effect in causing much more severe Dyf (Fig. 3 C). Further analysis indicated that the abnormal bulblike accumulations of IFT-B components, BBS proteins, and the OSM-3 motor in *arl-13* mutants were significantly rescued by the introduction of the *arl-3*–null allele (Fig. 3 E).

In middle segments of wild-type animals, IFT-A and IFT-B subcomplexes are transported together by kinesin-II and OSM-3 at the intermediate rate of 0.7 µm/s. According to our measurements, the length of the phasmid cilia along which IFT particles move at 0.7 µm/s is ~2.2 µm (Fig. 3 F). In *arl-13* mutants, this length decreases to ~1.5 µm. As expected, the length of middle segment can be partly rescued to ~2.0 µm in *arl-3; arl-13* double mutants (Fig. 3 F).

Ultrastructural defects in cilia of *arl-13* and *arl-3; arl-13* mutants

To investigate cilia deformations at the ultrastructural level, we used TEM to examine amphid cilia in various mutants (Fig. 4). Wild-type amphids contained 10 cilia bundled together (Fig. 4 A), whereas *arl-13* mutants had only six to eight distal segments, likely as a result of premature truncation of the distal segments of some cilia ($n = 8$; Fig. 4 B). The remaining distal segments contained normal microtubule singlets. Some truncations in the distal segments continued further, usually resulting in one to two missing middle segments in the worms we sectioned

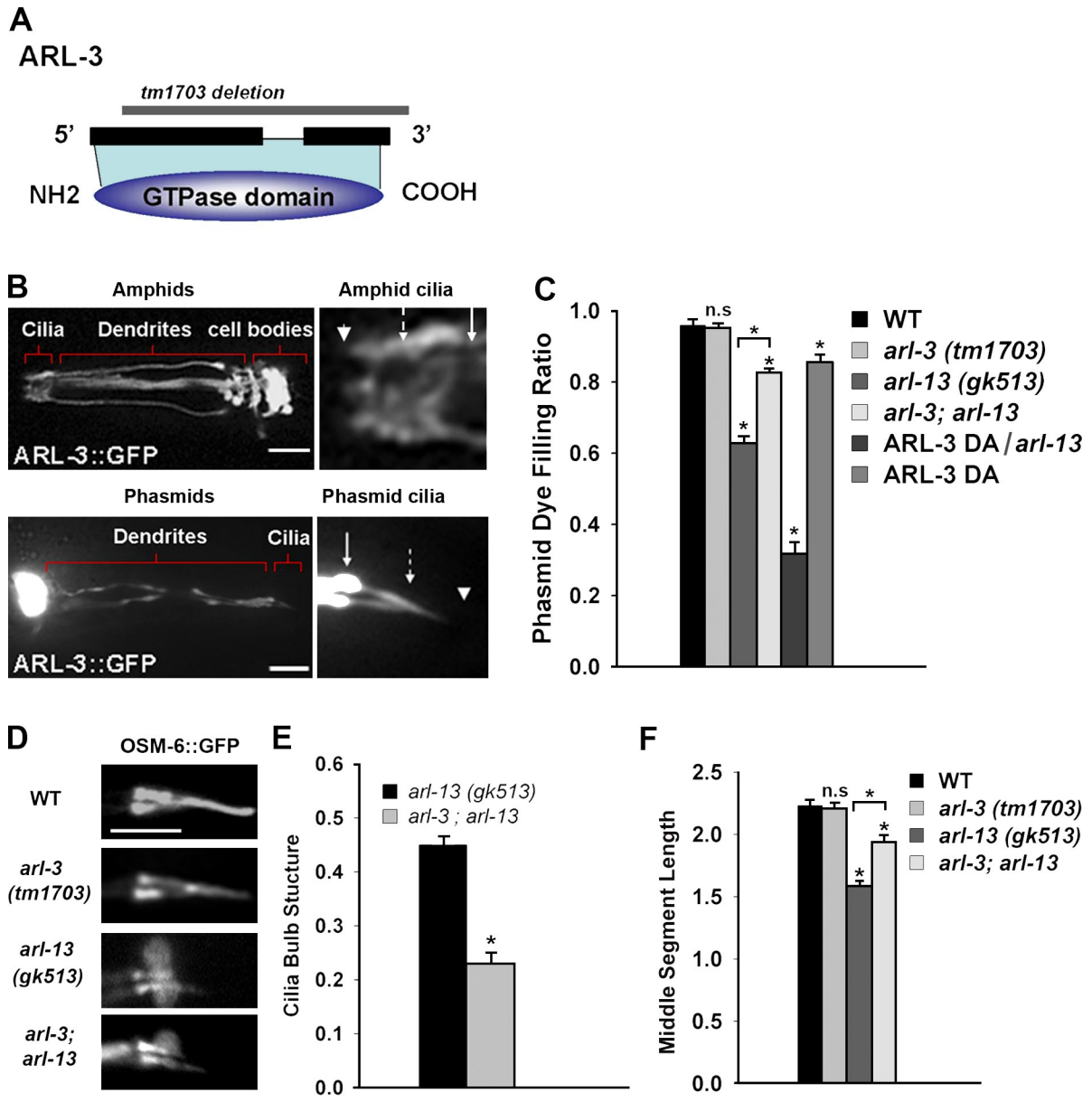

Figure 3. **ARL-3 depletion rescues cilia deformations in *arl-13* mutants.** (A) ARL-3 is a typical small GTPase. The *tm1703* allele removes most of the coding region, resulting in a null mutant. (B) In the adult worm, ARL-3::GFP localized to the cilium. Bars, 10 µm. (C) Depletion of ARL-3 partially rescued the phasmid cilia Dyf in *arl-13* mutants. However, overexpression of the DA ARL-3^{Q72L} mutant in an *arl-13* background caused a much more severe Dyf. (D) The morphology of phasmid cilia in *arl-3* mutants appeared normal. Bar, 5 µm. (E) ARL-3 depletion significantly reduced the occurrence of the bulblike structures observed in *arl-13* mutants. At least 100 animals were scored per genotype (~400 individual phasmid cilia were observed). (F) Middle segment length was also partially restored in *arl-3; arl-13* double mutants. At least 50 individual phasmid cilia were observed for each genotype. Solid arrows indicate the TZ, dashed arrows point to the approximate middle to distal segment transition points, and arrowheads mark the distal ends. WT, wild type. Statistical analysis was performed using a two-tailed paired Student's *t* test. *, $P < 0.001$. Error bars indicate SEM.

(Fig. 4 F). In contrast to the normal pattern in middle segments of nine peripheral doublets adjacent to the membrane, misplaced doublets were frequently seen in the ciliary lumen of *arl-13* mutants (Fig. 4, F and T, arrowheads), a phenomenon indicative of a disrupted axoneme architecture or microtubule: membrane connection.

Several other cilia deformations were observed in *arl-13* mutants. For example, an abnormal membrane distortion (seen in two of eight amphids of *arl-13* mutants; Fig. 4, F and R, black arrows) in middle segments may correlate with the bulblike structure observed in Fig. 2 C. Occasionally, we observed an increased number of outer doublets (14 rather than 9 doublets; Fig. 4 S) in a cilium, with most showing B-tubule seam breaks, and some doublets were seen in the ciliary lumen. This structure represents a fused cilium with misplaced doublets in the middle of the ciliary lumen. The *C. elegans* TZ typically contains a circular array of doublet microtubules with y links between the axoneme and ciliary membrane (Fig. 4, M–P, white arrows; Perkins et al., 1986). The number and morphology of amphid cilia in the TZ area of *arl-13* mutants were comparable with those of wild-type animals (Fig. 4, I, J, M, and N).

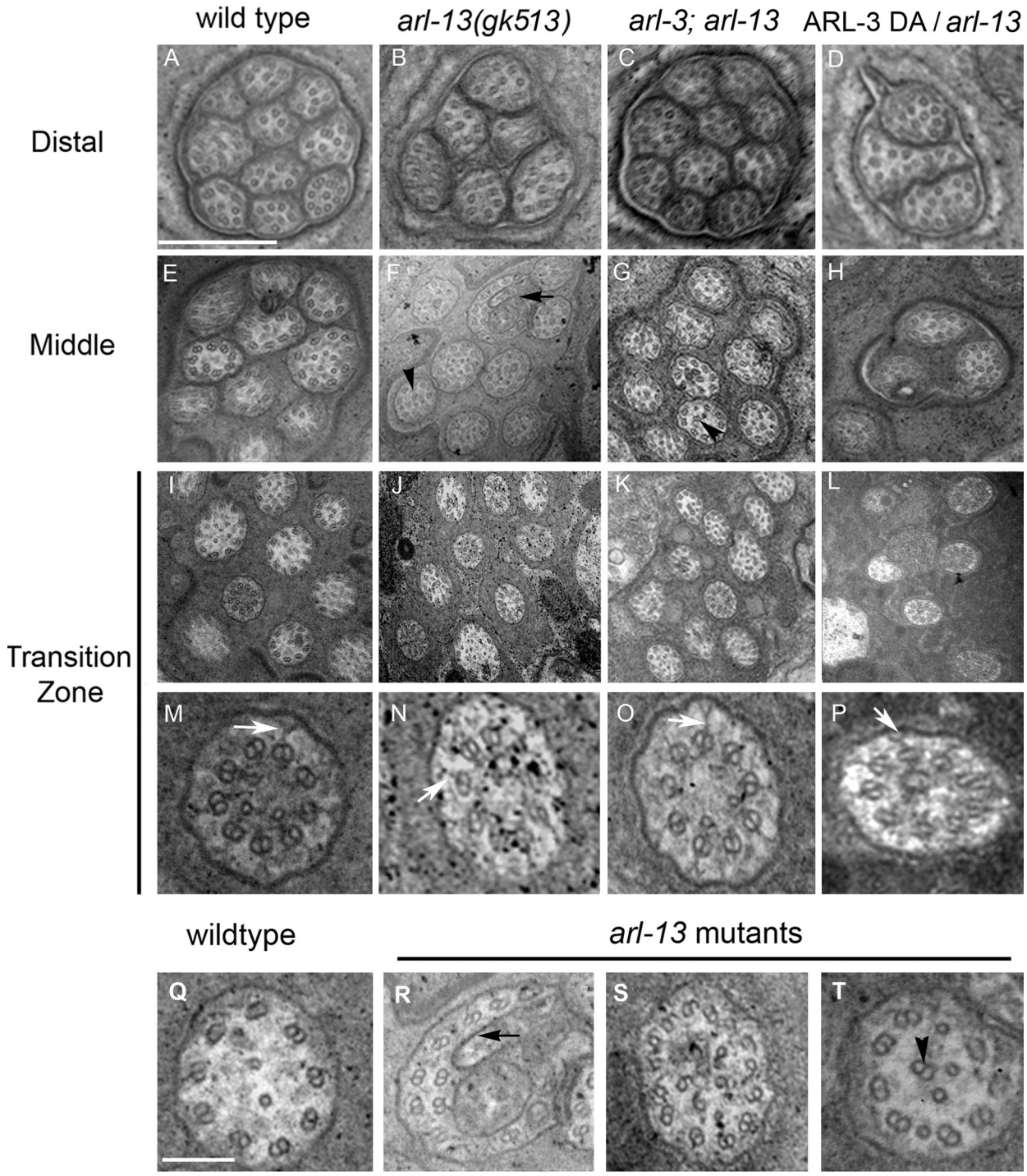

Figure 4. **ARL-3 depletion corrects the abnormal ultrastructure of *arl-13* amphid cilia.** TEM analyses of amphid cilia in wild-type (A, E, I, M, and Q), *arl-13* (B, F, J, N, and R–T), *arl-3; arl-13* (C, G, K, and O), and *ARL-3 DA; arl-13* (D, H, L, and P) animals are shown. The reduced cilia number (B and F) in *arl-13* single mutants could be restored to nearly the wild-type level in *arl-3; arl-13* double mutants (C and G). Overexpression of DA ARL-3 exacerbated the ciliogenesis defect of *arl-13* mutants (D, H, and L). TZs are characterized by the typical y links that connect the axoneme with the ciliary membrane (M–P, white arrows). Note that fewer cilia were seen in the TZ area in ARL-3 DA(*Xs*); *arl-13* animals (L), which indicate a more severe ciliogenesis defect. In all mutants, doublets were occasionally misplaced to the ciliary lumen (T, arrowhead). (R) An abnormal membrane structure that was occasionally found in *arl-13* mutants is shown. (S) A cilium in an *arl-13* mutant that exhibited an increased number of microtubule doublets surrounding the outer edge, most having a B-tubule seam break, is shown. This may represent a fused cilium. More than eight amphids were sectioned for each genotype. Black arrows indicate the abnormal membrane structure, and black arrowheads mark the misplaced doublet. Bars: (A–L) 0.5 μm; (M–T) 100 nm.

Consistent with our finding that ARL-3 depletion can rescue various ciliary deformations in *arl-13* mutants, the distal segments of *arl-3; arl-13* mutants were restored to 9–10 cilia, comparable with those of wild-type worms (Fig. 4 C). The abnormal membrane distortion (Fig. 4, F and R, arrows) and uncommon ciliary fusion with broken B-tubules were not

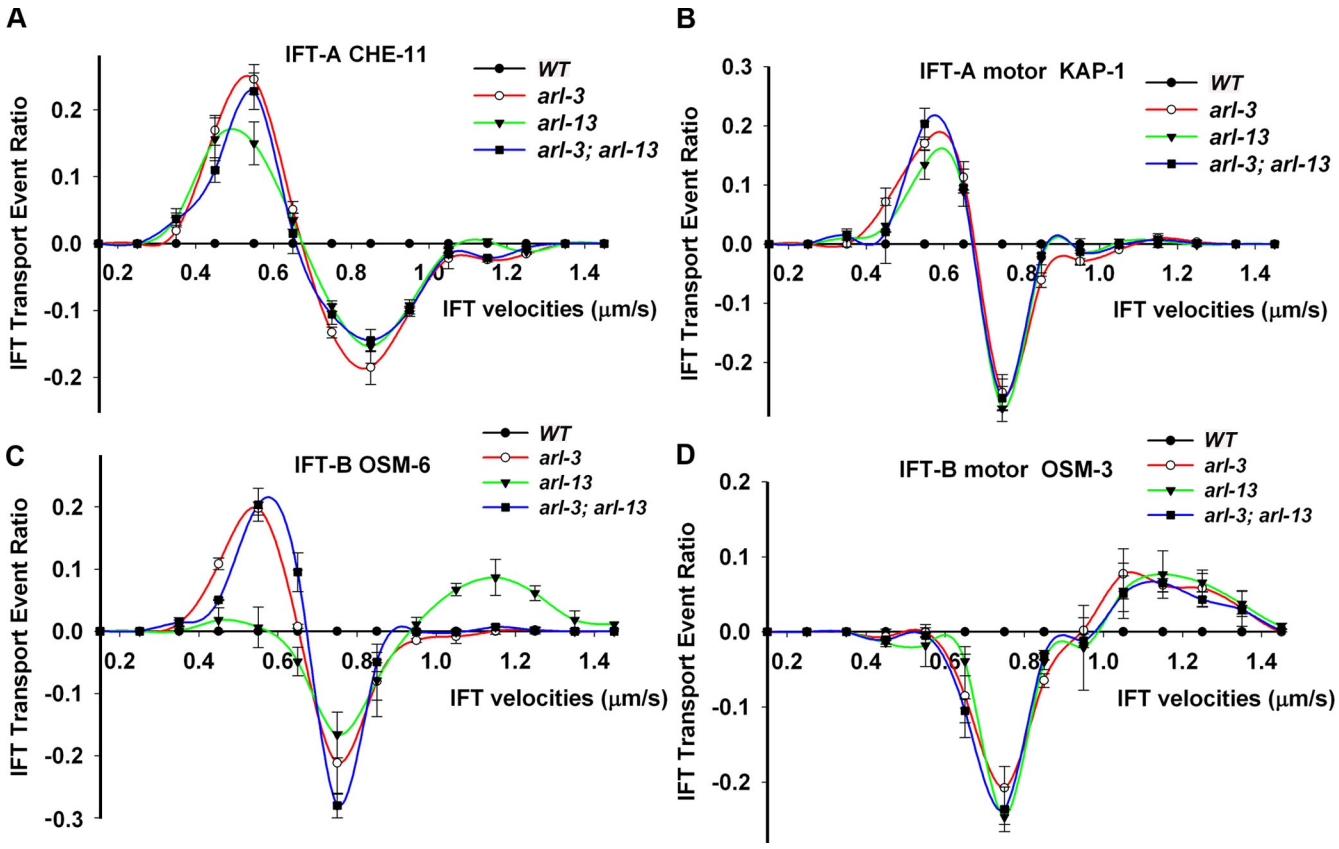

Figure 5. **ARL-13 and ARL-3 influence the integrity of the IFT macromolecular complex.** The IFT transport event ratios of GFP-tagged IFT proteins of wild-type (WT) animals were subtracted from those of *arl-3*(*tm1703*), *arl-13*(*gk513*), and *arl-3; arl-13* mutant animals. Positive value, negative value, and zero (y axis) represent the ratio of more, fewer, or an equal number of particles moving at a given specific velocity step (x axis) in mutants compared with wild-type animals. The simple spline curves in each figure were generated using SigmaPlot software (version 8; Systat Software, Inc.). For all mutants, the curves fit into a bimodal Gaussian distribution, with fewer particles moving at the normal rate of ∼0.7 µm/s (transport by kinesin-II and OSM-3 together) and more moving at either ∼0.5 (kinesin-II alone) or ∼1.3 µm/s (OSM-3 alone), depending on the IFT markers used in the analysis. IFT-A and IFT-B tended to dissociate and move with their own motors in *arl-13* mutants, whereas IFT-B tended to dissociate from OSM-3 and move together with IFT-A–kinesin-II in *arl-3* and *arl-3; arl-13* double mutants. Error bars indicate SEM.

detected in any examined *arl-3; arl-13* amphid cilium (n = 8), indicating a rescue effect. In accordance with the result that ARL-3 depletion could not completely rescue ciliogenesis defects in *arl-13* mutants, middle segments of *arl-3; arl-13* mutants possessed misplaced doublets in the ciliary lumen (Fig. 4 G, arrowhead).

However, overexpression of the ARL-3^{Q72L} DA mutant caused a much more severe ciliogenesis defect in *arl-13* animals. Only three to six middle and distal segments existed in the amphid cilia of ARL-3^{Q72L}(*Xs*); *arl-13* (Fig. 4, D and H). Unexpectedly, overexpression of ARL-3^{Q72L} DA also reduced the number of cilia in the TZ area (Fig. 4 L). Checking IFT markers in ARL-3^{Q72L}(*Xs*); *arl-13* mutants (Fig. S4 B) and examining TEM sections deeper into the dendrite region did not reveal mispositioned TZs or cilia. Thus, we conclude that some cilia are completely missing in ARL-3^{Q72L}(*Xs*); *arl-13* mutants. On the basis of these results and the observation that a significant amount of ARL-3 protein is cytosolic (Fig. 3 B), we propose that ARL-3 plays a role in a very early stage of ciliogenesis, possibly before TZ formation. Collectively, the TEM data complement our previous findings and support a model in which ARL-3 and ARL-13 act in opposite directions to regulate ciliogenesis.

ARL-3 depletion restores IFT-A–IFT-B binding in *arl-13* mutants

To gain a mechanistic insight into how ARL-3 depletion rescues ciliogenesis defects in *arl-13* mutants, we performed detailed IFT analysis on *arl-3* single and *arl-3; arl-13* double mutants. *arl-13* mutants showed a destabilized IFT complex (Fig. 2 E). To our surprise, a significant proportion of the IFT-A particles and kinesin-II motor moved at the slower rate of 0.5 µm/s in *arl-3*; *arl-13* mutants, as they did in *arl-13* mutants (Fig. 5, A and B). Moreover, the IFT-B component OSM-6 also tended to move at the slower 0.5 µm/s rate in *arl-3*; *arl-13* double mutants (Fig. 5 C). Interestingly, in contrast to all other IFT components tested, the OSM-3 motor tended to move at a faster rate of 1.3 µm/s in *arl-3; arl-13* mutants (Fig. 5 D). Thus, our data reveal that in *arl-3; arl-13* mutants, IFT-A and IFT-B subcomplexes move together and OSM-3 tends to dissociate from the IFT complex and move alone in the middle segments (see Fig. 7).

ARL-3 depletion does not rescue *arl-13* ciliogenesis defects by restoring the integrity of the entire IFT particle. Rather, the absence of ARL-3 destabilizes the association between IFT-B and the OSM-3 motor, which indirectly restores binding between

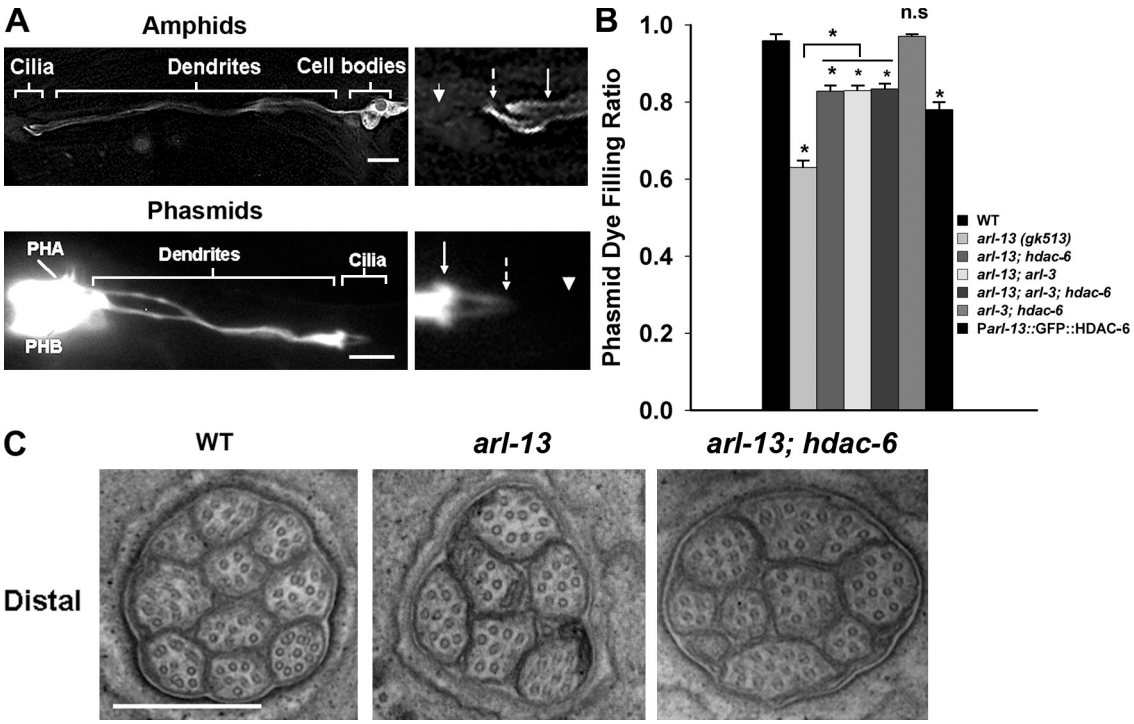

Figure 6. **ARL-3 and the deacetylase HDAC6 act in the same genetic pathway to regulate ciliogenesis.** (A) In the adult, GFP::HDAC6 located to the cilium, dendrite, and cell body. Note that most GFP::HDAC6 was detected along the middle segment in phasmid cilia. Solid arrows indicate the TZs, dashed arrows point to the approximate middle to distal segment transition points, and arrowheads mark the distal ends. Bars, 10 µm. (B) *arl-3* and *hdac6* act in the same genetic pathway to rescue the ciliogenesis defect in *arl-13* mutants. Overexpression of GFP::HDAC6 caused Dyf in wild-type (WT) animals. At least 100 animals were scored per genotype (~400 individual phasmid cilia were observed). (C) Amphid cilia were partially restored in *hdac6; arl-13* double mutants. For distal segments, 10 cilia were usually visualized in wild-type animals, six cilia in *arl-13* mutants, and nine cilia in *hdac6; arl-13* double mutants. Eight amphids were sectioned for each genotype. Bar, 0.5 µm. Statistical analysis was performed using a two-tailed paired Student's *t* test. *, $P < 0.001$. PHA and PHB indicate the cell bodies of two phasmid neurons. Error bars indicate SEM.

IFT-A and IFT-B subcomplexes. A similar scenario exists in *bbs* mutants. In *bbs* single mutants, IFT-A and IFT-B subcomplexes separate, but in *bbs*; *osm-3* double mutants, the subcomplexes move together by kinesin-II alone because of the absence of a dragging force generated by the faster OSM-3 motor (Pan et al., 2006). To support this conclusion, we examined *arl-3* mutants and found that more IFT-A and IFT-B moved together at a slower rate, whereas more OSM-3 moved at a faster rate (Fig. 5). In all mutants examined, the anterograde movement in distal segments and the retrograde movement were unchanged (Table S1). Notably, although the IFT integrity in *arl-3; arl-13* is reminiscent of that in *arl-3*, the former still show Dyf phenotype. This finding indicates that compromised IFT integrity is not the sole explanation for the ciliogenesis defects in *arl-13* mutants.

ARL-3 regulates ciliogenesis via an HDAC6-dependent pathway

Few systematic analyses of the effectors of Arl GTPases have been undertaken. One mechanistic study linked Arl3 depletion to increased tubulin acetylation in HeLa cells (Zhou et al., 2006a). Two tubulin deacetylases, HDAC6 and SIRT2, were characterized recently (Hubbert et al., 2002; North et al., 2003). Notably, HDAC6 physically interacts with a BBSome subunit, BBIP10, and is involved in BBIP10-dependent cytoplasmic tubulin acetylation (Loktev et al., 2008). To investigate whether ARL-3 and HDAC6 function in the same pathway to regulate ciliogenesis, we characterized the *C. elegans* HDAC6 homologue F41H10.6 (hereafter termed HDAC6). The *C. elegans hdac6* gene has one available mutant allele, *ok3203*, which removes ~400 bp of coding sequence and may result in a prematurely terminated protein or alternatively spliced products. *hdac6* mutants are superficially wild type and possess normal cilia on the basis of dye-filling experiments. *hdac6* gene expression was detected in ciliated amphids and phasmids, nerve cords, intestine, and pharynx (Fig. S3). In ciliated neurons, the GFP::HDAC6 signal is diffuse in the cell body, axon, dendrite, and cilium. Interestingly, GFP::HDAC6 is retained predominantly in the middle segment, like ARL-13::GFP (Fig. 6 A).

We then generated *arl-3; hdac6* double-, *arl-13; hdac6* double-, and *arl-3; arl-13; hdac6* triple-mutant animals. *arl-3; hdac6* double mutants were normal in the dye-filling assay. As shown in Fig. 6 B, the *hdac6* allele can rescue the ciliogenesis defect in *arl-13* to a similar extent as the *arl-3* allele. We next asked whether *hdac6* and *arl-3* act in the same genetic pathway to correct the ciliogenesis defects in *arl-13* mutants. Epistasis analysis is commonly used to assess genetic interactions among several genes. We reasoned that if *arl-3* and *hdac6* act independently or redundantly, we would observe an additive rescue effect in *arl-3; hdac6; arl-13* triple mutants. A dye-filling assay showed that the rescue effect in *arl-3; hdac6; arl-13* triple mutants is comparable with that in *arl-3; arl-13* or *hdac6; arl-13* double mutants, suggesting that *arl-3* and

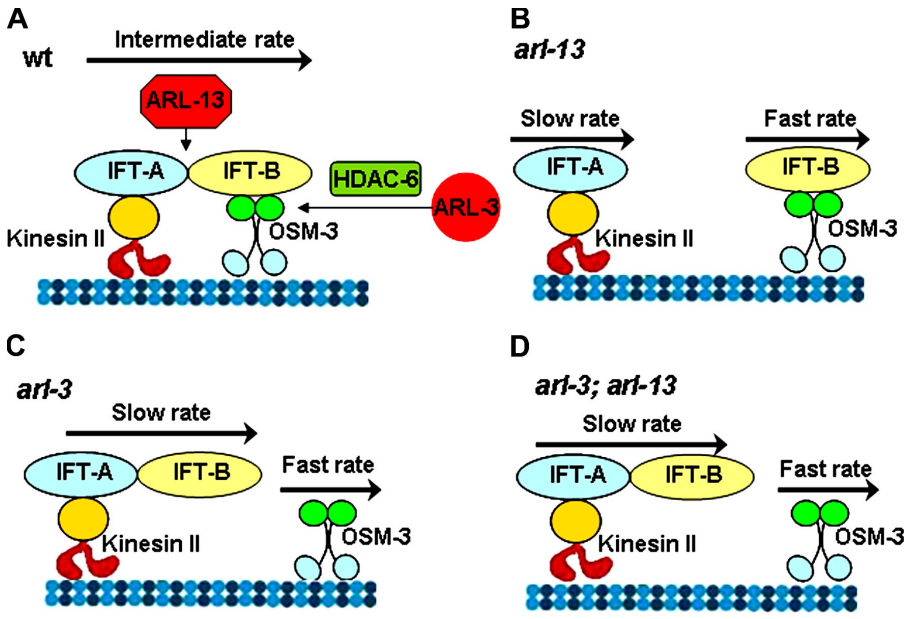

Figure 7. **Schematic model of ARL involvement in the regulation of IFT stability.** (A) In wild-type (wt) cilia, ARL-13 and ARL-3 stabilize the IFT complex. The holding force between IFT-A and IFT-B is counterbalanced by the dragging force generated by fast-moving OSM-3 motors and slow-moving kinesin-II motors. OSM-3 and kinesin-II coordinate the movement of IFT particles at an intermediate rate. (B) Because of the attenuated association between IFT-A and IFT-B in *arl-13* mutants, the holding force is smaller than the dragging force. Some IFT-A and IFT-B are dissociated and moved by their own motors at slow or fast rates. (C and D) In both *arl-3* single (C) and *arl-3; arl-13* double (D) mutants, the weakened connection between OSM-3 and the IFT-B subcomplex reduces the dragging force that OSM-3 exerts on the rest of the IFT complex, and thereby indirectly restores the binding efficiency of IFT-A and IFT-B.

hdac6 act in the same genetic pathway to regulate cilia formation. Furthermore, TEM analyses confirmed that the distal amphid cilia number can be restored to the wild-type level in *hdac6; arl-13* double mutants (n = 8; Fig. 6 C). Similar to ARL-3 DA overexpression, HDAC6 overexpression could cause Dyf (Fig. 6 B). Therefore, our data reveal that the previously reported, microtubule-associated deacetylase HDAC6 plays a novel role in the ciliogenesis pathway regulated by the small GTPase ARL-3.

Collectively, our data support the working model that ARL-13 and ARL-3, although not moved along the cilium, play novel roles in coordinating IFT (Fig. 7). Specifically, we propose that ARL-13 acts to enhance the binding force between IFT-A and IFT-B subcomplexes, and ARL-3 functions in an HDAC6–dependent manner to regulate the association between IFT-B and the OSM-3 motor. The absence of ARL-13 produces a destabilized IFT complex, which can be pulled apart into separate IFT-A–kinesin-II and IFT-B–OSM-3 particles by the dragging force generated between faster-moving OSM-3 motors and slower-moving kinesin-II motors. In *arl-3* single and *arl-3; arl-13* double mutants, the significantly attenuated association between IFT-B and OSM-3 reduces the dragging force and indirectly restores the binding efficiency of IFT-A and IFT-B subcomplexes.

Discussion

Considerable interest exists in further defining the molecular pathways that lead to ciliopathies. Exploring the in vivo molecular mechanisms of conserved disease genes in a simple *C. elegans* model system has helped advance our understanding of the pathophysiologies of many ciliopathies, such as autosomal dominant polycystic kidney disease, Merkel–Gruber syndrome, nephronophthisis, and BBS syndromes (Haycraft et al., 2001; Fan et al., 2004; Barr, 2005; Badano et al., 2006; Jauregui et al., 2008; Williams et al., 2008; Bialas et al., 2009).

The cilia-related phenotypes of *arl-3* and *arl-13* mutants reported in this study are quite reminiscent of those in other organisms. For example, in *L. donovani*, a DA form of ARL-3 (LdARL-3A) caused a truncated flagellum, whereas the dominant-negative form did not affect flagellum biogenesis. *Arl3*$^{(-/-)}$ mice show apparently normal ciliary structure but abnormal ciliary protein transport in photoreceptors. Zebrafish *Arl13b*/*scorpion* mutants show abnormal cilia formation (Sun et al., 2004), and *Arl13b*$^{(-/-)}$ mice possess shortened cilia with a specific B-tubule closing defect that is similar to what we observed in *arl-13* worms (Fig. 4 S; Caspary et al., 2007).

Effectors of ARL-3 and ARL-13

Although IFT integrity in *arl-3; arl-13* mutants was restored to a similar state as that in *arl-3* mutants (Fig. 5; and Fig. 7, C and D), *arl-3; arl-13* mutants still display mild ciliogenesis defects. One hypothesis to explain this observation is that the effectors of ARL-13 may have two distinct functions: one related to regulating IFT integrity and the other a non-IFT–related function, such as membrane–microtubule architecture. This hypothesis is supported by the observation with TEM that *arl-3; arl-13* mutants possess misplaced doublets. ARL-3 depletion indirectly restores IFT but is not able to correct other non-IFT–related ciliogenesis defects; therefore, we did not see a complete rescue effect for the *arl-3; arl-13* double mutants.

The cellular effectors of ARL-3 and ARL-13 are poorly understood. However, experiments on ARL mutants with altered GTP-binding capacity indicate that normal ciliogenesis requires the GTPase activities of both ARL-3 and ARL-13 (Fig. 2 A and Fig. 3 C). Identification of the putative GTPase exchange factor and GTPase-activating protein that bind to ARL-3 and ARL-13 will be critical to fully dissect their roles in cilia biogenesis and IFT regulation. Remarkably, the proposed roles of ARL-13 and ARL-3 in IFT regulation resemble the roles proposed for the BBSome and DYF-1 in this system (Ou et al., 2005). It would be informative to study how ARLs, BBS

proteins, and DYF-1 converge in the same pathway to regulate ciliogenesis and IFT.

The C-terminal PRD of ARL-13 is indispensable for its specific targeting to the doublet segment of the cilium. The PRD and its major interacting domain, SH3 (Src homology 3), have been shown to be involved in various protein–protein interactions. Interestingly, a PRD is found in many microtubule-associated proteins such as MAP2, τ, and MAP4 and is required for the activities of microtubule-associated proteins in microtubule binding and assembly (West et al., 1991; Kanai et al., 1992; Ferralli et al., 1994; Tokuraku et al., 1999). Additionally, the PRD of the GTPase dynamin regulates its effector binding and microtubule association (Gout et al., 1993; Hamao et al., 2009). In our experiments, overexpression of the ARL-13 PRD domain induced a dominant-negative effect on ciliogenesis (Fig. 2 A). Overexpression of the ARL-13 NT truncation, which lacks the PRD domain but contains the entire GTPase domain, could also cause Dyf in the phasmid cilia of wild-type animals. Similarly, the *arl-13*(*tm2322*) allele is an in-frame deletion and encodes a truncated ARL-13 protein that lacks the PRD domain but retains the intact GTPase domain (Fig. 1 A). Both *arl-13*(*gk513*) and *arl-13*(*tm2322*) animals show comparable ciliogenesis defects (unpublished data). Remarkably, contrary to our observation that none of the IFT reporters interfere with ciliogenesis in *arl-13* (*gk513*) mutants, IFT transgene overexpression can enhance the ciliogenesis defect of *arl-13*(*tm2322*) mutant cilia (Cevik et al., 2010). These findings provide support for the view that the PRD domain of ARL-13 is critical for both ciliary targeting and cilia formation, and loss of the PRD domain could result in a truncated ARL-13 protein with deregulated GTPase activity. Thus, characterization of the ciliary proteins that bind the ARL-13 PRD domain is of great interest.

What are HDAC6's substrates in ciliogenesis?

We demonstrate in this study that ARL-3 acts through the deacetylase HDAC6 to regulate cilia formation in *C. elegans*. HDAC6 deacetylates not only histones (Grozinger et al., 1999) but also α-tubulin (Hubbert et al., 2002), Hsp90 (Kovacs et al., 2005), and cortactin (Zhang et al., 2007). Inhibition of HDAC6 enzymatic activity causes increased transport of the kinesin-1 cargo complex along microtubules in neuronal cells (Reed et al., 2006). Reminiscent of our findings, activation of HDAC6 can promote cilia disassembly, and loss of HDAC6 activity selectively stabilizes cilia in human retinal epithelial cells (Pugacheva et al., 2007).

Currently, HDAC6 is thought to regulate microtubule-dependent processes by deacetylating α-tubulin. However, this model is inaccurate for the *C. elegans* ciliogenesis pathway because MEC-12, the only α-tubulin capable of being acetylated, is not expressed in ciliated amphids and phasmids (Fukushige et al., 1999). Another HDAC6 substrate, Hsp90, was shown to associate with β-tubulin and may be involved in stabilizing tubulin polymerization in cilia (Takaki et al., 2007). However, worms with a null allele of *daf-21*, the *C. elegans* homologue of *Hsp90*, possess normal cilia in our analysis (unpublished data). These data rule out α-tubulin and Hsp90 as candidate HDAC6 substrates during ciliogenesis in *C. elegans*. On the basis of our model, we propose that HDAC6 deacetylates an unknown adaptor protein in IFT-B–OSM-3 subcomplexes.

Non-IFT–related roles for ARL-3 in cilia formation

ARL-3 appears to have non-IFT–related functions in cilia. Overexpression of DA ARL-3 in *arl-13* mutants produces a new defect in that some cilia are missing in the TZ area (Fig. 4 L). This striking phenotype is not the result of compromised IFT in middle segments because previous TEM analyses showed that TZs can form normally in all IFT mutants examined (Perkins et al., 1986). Because *C. elegans* and vertebrate ARL-3s are cytosolic (Fig. 3 B; Behnia et al., 2004; Setty et al., 2004) and at least one IFT protein (IFT20) moves between the Golgi apparatus and adjacent basal body (Follit et al., 2006), the overexpression of DA ARL-3 could interfere with normal protein transport between the Golgi and TZ. When this interference is combined with the already compromised ciliogenesis of *arl-13* mutants, the normal TZ formation could be disrupted. A possible ARL-3 effector in this pathway is the retinitis pigmentosa 2 (RP2) protein. In the mammalian retina, RP2 interacts with GTP-bound Arl3 and functions as a GTPase-activating protein (Grayson et al., 2002; Veltel et al., 2008). K08D12.2, the *C. elegans* homologue of RP2, is expressed exclusively in ciliated cells and localizes specifically around TZs but not along the axoneme (Blacque et al., 2005). It would be informative to examine whether ARL-3 and RP2 form a functional complex and play a role in the early stage of ciliogenesis.

In conclusion, our findings reveal a novel coordination mechanism for ARL-13 and ARL-3 in cilia formation. Considering the strikingly similar mutant phenotypes across different species, the ciliary roles of ARL-13 and ARL-3 identified in this study are probably evolutionarily conserved in other organisms. The next challenge is to elucidate the effectors of ARL-13 and ARL-3 and the substrates of HDAC6 involved in regulating ciliogenesis.

Materials and methods

C. elegans mutant alleles and strains

Nematodes were raised using standard conditions described previously (Brenner, 1974). N2 worms represented the wild-type animals in all assays. All strains used in this paper are listed in Table S2.

Dye-filling assay

The stock DiI (2 mg/ml in dimethyl formamide; Invitrogen) was diluted 1:200 in M9. Worms were incubated in diluted dye for 1 h at room temperature. After incubation, the animals were washed at least three times with M9 and observed using a fluorescence microscope (M2Bio; Carl Zeiss, Inc.).

Microscopy

Animals were raised at 20°C and imaged using standard *C. elegans* slide mounts and a Plan Apochromat 60× 1.49 NA oil objective (Nikon) on an imaging microscope (TE 2000-U; Nikon).

IFT measurement

We performed all IFT analyses in phasmids for easier observation. IFT motility was observed using a Plan Apochromat 100× 1.49 NA oil total internal reflection fluorescence objective (Nikon). In wild-type worms, the IFT velocities in phasmid cilia were identical to those reported in amphid cilia (Table S1). Motility stacks were recorded using a charge-coupled device camera (QuantEM 512SC; Roper Industries), and kymographs were produced

using MetaMorph software (MDS Analytical Technologies). Worms were anesthetized in a drop of M9 containing 10 mM levamisole, transferred to an agarose mount slide, and imaged immediately.

TEM

For TEM, worms were fixed in 2.5% glutaraldehyde in cacodylate buffer on ice. Heads were cut off, moved to fresh fixative, and held overnight at 4°C. Animals were rinsed in buffer and stained with 1% osmium tetroxide in cacodylate buffer for 1 h at 4°C. After embedding small groups of worms in agarose, the specimens were dehydrated and embedded in Embed812 resin according to the general procedures described previously (Hall, 1995). Thin sections were collected on a diamond knife and poststained before viewing on an electron microscope (JEM-1400; JEOL).

Online supplemental material

Fig. S1 shows that *arl-3* and *arl-13* are expressed exclusively in ciliated cells. Fig. S2 shows that ARL-3 and ARL-13 show no IFT motility. Fig. S3 shows that *hdac6* is expressed in ciliated cells. Fig. S4 shows that ARL-3 localizes normally in *arl-13* mutants, and TZ morphology appears normal in ARL-3^{Q72L}(*Xs*); *arl-13* animals. Table S1 shows IFT velocities of various IFT markers in *arl-3* and *arl-13* single mutants and *arl-3; arl-13* double mutants. Table S2 shows all of the strains used in this study. Online supplemental material is available at http://www.jcb.org/cgi/content/full/jcb.200912001/DC1.

We thank the *Caenorhabditis* Genetics Center, the Japanese Bioresource Project, and Drs. Jonathan Scholey, Michel Leroux, and Maureen Barr for strains. We also thank Drs. Maureen Barr, Peter Harris, Vicente Torres, Nicholas LaRusso, Jeffery Salisbury, and Ms. Natalia Morsci for helpful discussions.

This research was funded by the Polycystic Kidney Disease (PKD) Foundation Young Investigator Award (grant 04YI09a to J. Hu). J. Hu is also supported by a FULK Career Development award, the Zell PKD Disease Research Fund, and the Upjohn PKD Research Fund from Mayo Clinic.

Submitted: 1 December 2009
Accepted: 13 May 2010

References

Avidor-Reiss, T., A.M. Maer, E. Koundakjian, A. Polyanovsky, T. Keil, S. Subramaniam, and C.S. Zuker. 2004. Decoding cilia function: defining specialized genes required for compartmentalized cilia biogenesis. *Cell.* 117:527–539. doi:10.1016/S0092-8674(04)00412-X

Badano, J.L., N. Mitsuma, P.L. Beales, and N. Katsanis. 2006. The ciliopathies: an emerging class of human genetic disorders. *Annu. Rev. Genomics Hum. Genet.* 7:125–148. doi:10.1146/annurev.genom.7.080505.115610

Barr, M.M. 2005. *Caenorhabditis elegans* as a model to study renal development and disease: sexy cilia. *J. Am. Soc. Nephrol.* 16:305–312. doi:10.1681/ASN.2004080645

Behnia, R., B. Panic, J.R. Whyte, and S. Munro. 2004. Targeting of the Arf-like GTPase Arl3p to the Golgi requires N-terminal acetylation and the membrane protein Sys1p. *Nat. Cell Biol.* 6:405–413. doi:10.1038/ncb1120

Bialas, N.J., P.N. Inglis, C. Li, J.F. Robinson, J.D. Parker, M.P. Healey, E.E. Davis, C.D. Inglis, T. Toivonen, D.C. Cottell, et al. 2009. Functional interactions between the ciliopathy-associated Meckel syndrome 1 (MKS1) protein and two novel MKS1-related (MKSR) proteins. *J. Cell Sci.* 122:611–624. doi:10.1242/jcs.028621

Blacque, O.E., E.A. Perens, K.A. Boroevich, P.N. Inglis, C. Li, A. Warner, J. Khattra, R.A. Holt, G. Ou, A.K. Mah, et al. 2005. Functional genomics of the cilium, a sensory organelle. *Curr. Biol.* 15:935–941. doi:10.1016/j.cub.2005.04.059

Brenner, S. 1974. The genetics of *Caenorhabditis elegans*. *Genetics.* 77:71–94.

Cantagrel, V., J.L. Silhavy, S.L. Bielas, D. Swistun, S.E. Marsh, J.Y. Bertrand, S. Audollent, T. Attié-Bitach, K.R. Holden, W.B. Dobyns, et al; International Joubert Syndrome Related Disorders Study Group. 2008. Mutations in the cilia gene ARL13B lead to the classical form of Joubert syndrome. *Am. J. Hum. Genet.* 83:170–179. doi:10.1016/j.ajhg.2008.06.023

Caspary, T., C.E. Larkins, and K.V. Anderson. 2007. The graded response to Sonic Hedgehog depends on cilia architecture. *Dev. Cell.* 12:767–778. doi:10.1016/j.devcel.2007.03.004

Cevik, S., Y. Hori, O.I. Kaplan, K. Kida, T. Toivenon, C. Foley-Fisher, D. Cottell, T. Katada, K. Kontani, and O.E. Blacque. 2010. Joubert syndrome Arl13b functions at ciliary membranes and stabilizes protein transport in *Caenorhabditis elegans*. *J. Cell Biol.* 188:953–969. doi:10.1083/jcb.200908133

Cuvillier, A., F. Redon, J.C. Antoine, P. Chardin, T. DeVos, and G. Merlin. 2000. LdARL-3A, a *Leishmania* promastigote-specific ADP-ribosylation factor-like protein, is essential for flagellum integrity. *J. Cell Sci.* 113:2065–2074.

D'Souza-Schorey, C., and P. Chavrier. 2006. ARF proteins: roles in membrane traffic and beyond. *Nat. Rev. Mol. Cell Biol.* 7:347–358. doi:10.1038/nrm1910

Duldulao, N.A., S. Lee, and Z. Sun. 2009. Cilia localization is essential for in vivo functions of the Joubert syndrome protein Arl13b/Scorpion. *Development.* 136:4033–4042. doi:10.1242/dev.036350

Eley, L., L.M. Yates, and J.A. Goodship. 2005. Cilia and disease. *Curr. Opin. Genet. Dev.* 15:308–314. doi:10.1016/j.gde.2005.04.008

Fan, Y., M.A. Esmail, S.J. Ansley, O.E. Blacque, K. Boroevich, A.J. Ross, S.J. Moore, J.L. Badano, H. May-Simera, D.S. Compton, et al. 2004. Mutations in a member of the Ras superfamily of small GTP-binding proteins causes Bardet-Biedl syndrome. *Nat. Genet.* 36:989–993. doi:10.1038/ng1414

Ferralli, J., T. Doll, and A. Matus. 1994. Sequence analysis of MAP2 function in living cells. *J. Cell Sci.* 107:3115–3125.

Fliegauf, M., T. Benzing, and H. Omran. 2007. When cilia go bad: cilia defects and ciliopathies. *Nat. Rev. Mol. Cell Biol.* 8:880–893. doi:10.1038/nrm2278

Follit, J.A., R.A. Tuft, K.E. Fogarty, and G.J. Pazour. 2006. The intraflagellar transport protein IFT20 is associated with the Golgi complex and is required for cilia assembly. *Mol. Biol. Cell.* 17:3781–3792. doi:10.1091/mbc.E06-02-0133

Fukushige, T., Z.K. Siddiqui, M. Chou, J.G. Culotti, C.B. Gogonea, S.S. Siddiqui, and M. Hamelin. 1999. MEC-12, an alpha-tubulin required for touch sensitivity in *C. elegans*. *J. Cell Sci.* 112:395–403.

Gillingham, A.K., and S. Munro. 2007. The small G proteins of the Arf family and their regulators. *Annu. Rev. Cell Dev. Biol.* 23:579–611. doi:10.1146/annurev.cellbio.23.090506.123209

Gout, I., R. Dhand, I.D. Hiles, M.J. Fry, G. Panayotou, P. Das, O. Truong, N.F. Totty, J. Hsuan, G.W. Booker, et al. 1993. The GTPase dynamin binds to and is activated by a subset of SH3 domains. *Cell.* 75:25–36.

Grayson, C., F. Bartolini, J.P. Chapple, K.R. Willison, A. Bhamidipati, S.A. Lewis, P.J. Luthert, A.J. Hardcastle, N.J. Cowan, and M.E. Cheetham. 2002. Localization in the human retina of the X-linked retinitis pigmentosa protein RP2, its homologue cofactor C and the RP2 interacting protein Arl3. *Hum. Mol. Genet.* 11:3065–3074. doi:10.1093/hmg/11.24.3065

Grozinger, C.M., C.A. Hassig, and S.L. Schreiber. 1999. Three proteins define a class of human histone deacetylases related to yeast Hda1p. *Proc. Natl. Acad. Sci. USA.* 96:4868–4873. doi:10.1073/pnas.96.9.4868

Hall, D.H. 1995. Electron microscopy and three-dimensional image reconstruction. *Methods Cell Biol.* 48:395–436. doi:10.1016/S0091-679X(08)61397-7

Hamao, K., M. Morita, and H. Hosoya. 2009. New function of the proline rich domain in dynamin-2 to negatively regulate its interaction with microtubules in mammalian cells. *Exp. Cell Res.* 315:1336–1345. doi:10.1016/j.yexcr.2009.01.025

Haycraft, C.J., P. Swoboda, P.D. Taulman, J.H. Thomas, and B.K. Yoder. 2001. The *C. elegans* homolog of the murine cystic kidney disease gene Tg737 functions in a ciliogenic pathway and is disrupted in osm-5 mutant worms. *Development.* 128:1493–1505.

Hedgecock, E.M., J.G. Culotti, J.N. Thomson, and L.A. Perkins. 1985. Axonal guidance mutants of *Caenorhabditis elegans* identified by filling sensory neurons with fluorescein dyes. *Dev. Biol.* 111:158–170. doi:10.1016/0012-1606(85)90443-9

Hubbert, C., A. Guardiola, R. Shao, Y. Kawaguchi, A. Ito, A. Nixon, M. Yoshida, X.F. Wang, and T.P. Yao. 2002. HDAC6 is a microtubule-associated deacetylase. *Nature.* 417:455–458. doi:10.1038/417455a

Insinna, C., N. Pathak, B. Perkins, I. Drummond, and J.C. Besharse. 2008. The homodimeric kinesin, Kif17, is essential for vertebrate photoreceptor sensory outer segment development. *Dev. Biol.* 316:160–170. doi:10.1016/j.ydbio.2008.01.025

Insinna, C., M. Humby, T. Sedmak, U. Wolfrum, and J.C. Besharse. 2009. Different roles for KIF17 and kinesin II in photoreceptor development and maintenance. *Dev. Dyn.* 238:2211–2222. doi:10.1002/dvdy.21956

Jauregui, A.R., K.C. Nguyen, D.H. Hall, and M.M. Barr. 2008. The *Caenorhabditis elegans* nephrocystins act as global modifiers of cilium structure. *J. Cell Biol.* 180:973–988. doi:10.1083/jcb.200707090

Jenkins, P.M., T.W. Hurd, L. Zhang, D.P. McEwen, R.L. Brown, B. Margolis, K.J. Verhey, and J.R. Martens. 2006. Ciliary targeting of olfactory CNG channels requires the CNGB1b subunit and the kinesin-2 motor protein, KIF17. *Curr. Biol.* 16:1211–1216. doi:10.1016/j.cub.2006.04.034

Kanai, Y., J. Chen, and N. Hirokawa. 1992. Microtubule bundling by tau proteins in vivo: analysis of functional domains. *EMBO J.* 11:3953–3961.

Kovacs, J.J., P.J. Murphy, S. Gaillard, X. Zhao, J.T. Wu, C.V. Nicchitta, M. Yoshida, D.O. Toft, W.B. Pratt, and T.P. Yao. 2005. HDAC6 regulates

Hsp90 acetylation and chaperone-dependent activation of glucocorticoid receptor. *Mol. Cell.* 18:601–607. doi:10.1016/j.molcel.2005.04.021

Li, J.B., J.M. Gerdes, C.J. Haycraft, Y. Fan, T.M. Teslovich, H. May-Simera, H. Li, O.E. Blacque, L. Li, C.C. Leitch, et al. 2004. Comparative genomics identifies a flagellar and basal body proteome that includes the BBS5 human disease gene. *Cell.* 117:541–552. doi:10.1016/S0092-8674(04)00450-7

Lin, F., T. Hiesberger, K. Cordes, A.M. Sinclair, L.S. Goldstein, S. Somlo, and P. Igarashi. 2003. Kidney-specific inactivation of the KIF3A subunit of kinesin-II inhibits renal ciliogenesis and produces polycystic kidney disease. *Proc. Natl. Acad. Sci. USA.* 100:5286–5291. doi:10.1073/pnas.0836980100

Loktev, A.V., Q. Zhang, J.S. Beck, C.C. Searby, T.E. Scheetz, J.F. Bazan, D.C. Slusarski, V.C. Sheffield, P.K. Jackson, and M.V. Nachury. 2008. A BBSome subunit links ciliogenesis, microtubule stability, and acetylation. *Dev. Cell.* 15:854–865. doi:10.1016/j.devcel.2008.11.001

Marszalek, J.R., X. Liu, E.A. Roberts, D. Chui, J.D. Marth, D.S. Williams, and L.S. Goldstein. 2000. Genetic evidence for selective transport of opsin and arrestin by kinesin-II in mammalian photoreceptors. *Cell.* 102:175–187. doi:10.1016/S0092-8674(00)00023-4

North, B.J., B.L. Marshall, M.T. Borra, J.M. Denu, and E. Verdin. 2003. The human Sir2 ortholog, SIRT2, is an NAD+-dependent tubulin deacetylase. *Mol. Cell.* 11:437–444. doi:10.1016/S1097-2765(03)00038-8

Ou, G., O.E. Blacque, J.J. Snow, M.R. Leroux, and J.M. Scholey. 2005. Functional coordination of intraflagellar transport motors. *Nature.* 436:583–587. doi:10.1038/nature03818

Pan, X., G. Ou, G. Civelekoglu-Scholey, O.E. Blacque, N.F. Endres, L. Tao, A. Mogilner, M.R. Leroux, R.D. Vale, and J.M. Scholey. 2006. Mechanism of transport of IFT particles in *C. elegans* cilia by the concerted action of kinesin-II and OSM-3 motors. *J. Cell Biol.* 174:1035–1045. doi:10.1083/jcb.200606003

Parisi, M.A. 2009. Clinical and molecular features of Joubert syndrome and related disorders. *Am. J. Med. Genet. C. Semin. Med. Genet.* 151C:326–340. doi:10.1002/ajmg.c.30229

Pazour, G.J., and J.L. Rosenbaum. 2002. Intraflagellar transport and cilia-dependent diseases. *Trends Cell Biol.* 12:551–555. doi:10.1016/S0962-8924(02)02410-8

Pazour, G.J., N. Agrin, J. Leszyk, and G.B. Witman. 2005. Proteomic analysis of a eukaryotic cilium. *J. Cell Biol.* 170:103–113. doi:10.1083/jcb.200504008

Perkins, L.A., E.M. Hedgecock, J.N. Thomson, and J.G. Culotti. 1986. Mutant sensory cilia in the nematode *Caenorhabditis elegans*. *Dev. Biol.* 117:456–487. doi:10.1016/0012-1606(86)90314-3

Pugacheva, E.N., S.A. Jablonski, T.R. Hartman, E.P. Henske, and E.A. Golemis. 2007. HEF1-dependent Aurora A activation induces disassembly of the primary cilium. *Cell.* 129:1351–1363. doi:10.1016/j.cell.2007.04.035

Reed, N.A., D. Cai, T.L. Blasius, G.T. Jih, E. Meyhofer, J. Gaertig, and K.J. Verhey. 2006. Microtubule acetylation promotes kinesin-1 binding and transport. *Curr. Biol.* 16:2166–2172. doi:10.1016/j.cub.2006.09.014

Rosenbaum, J.L., and G.B. Witman. 2002. Intraflagellar transport. *Nat. Rev. Mol. Cell Biol.* 3:813–825. doi:10.1038/nrm952

Scholey, J.M. 2008. Intraflagellar transport motors in cilia: moving along the cell's antenna. *J. Cell Biol.* 180:23–29. doi:10.1083/jcb.200709133

Schrick, J.J., P. Vogel, A. Abuin, B. Hampton, and D.S. Rice. 2006. ADP-ribosylation factor-like 3 is involved in kidney and photoreceptor development. *Am. J. Pathol.* 168:1288–1298. doi:10.2353/ajpath.2006.050941

Setty, S.R., T.I. Strochlic, A.H. Tong, C. Boone, and C.G. Burd. 2004. Golgi targeting of ARF-like GTPase Arl3p requires its Nalpha-acetylation and the integral membrane protein Sys1p. *Nat. Cell Biol.* 6:414–419. doi:10.1038/ncb1121

Signor, D., K.P. Wedaman, L.S. Rose, and J.M. Scholey. 1999. Two heteromeric kinesin complexes in chemosensory neurons and sensory cilia of *Caenorhabditis elegans*. *Mol. Biol. Cell.* 10:345–360.

Snow, J.J., G. Ou, A.L. Gunnarson, M.R. Walker, H.M. Zhou, I. Brust-Mascher, and J.M. Scholey. 2004. Two anterograde intraflagellar transport motors cooperate to build sensory cilia on *C. elegans* neurons. *Nat. Cell Biol.* 6:1109–1113. doi:10.1038/ncb1186

Sun, Z., A. Amsterdam, G.J. Pazour, D.G. Cole, M.S. Miller, and N. Hopkins. 2004. A genetic screen in zebrafish identifies cilia genes as a principal cause of cystic kidney. *Development.* 131:4085–4093. doi:10.1242/dev.01240

Takaki, E., M. Fujimoto, T. Nakahari, S. Yonemura, Y. Miyata, N. Hayashida, K. Yamamoto, R.B. Vallee, T. Mikuriya, K. Sugahara, et al. 2007. Heat shock transcription factor 1 is required for maintenance of ciliary beating in mice. *J. Biol. Chem.* 282:37285–37292. doi:10.1074/jbc.M704562200

Tokuraku, K., M. Katsuki, H. Nakagawa, and S. Kotani. 1999. A new model for microtubule-associated protein (MAP)-induced microtubule assembly. The Pro-rich region of MAP4 promotes nucleation of microtubule assembly in vitro. *Eur. J. Biochem.* 259:158–166. doi:10.1046/j.1432-1327.1999.00019.x

Veltel, S., A. Kravchenko, S. Ismail, and A. Wittinghofer. 2008. Specificity of Arl2/Arl3 signaling is mediated by a ternary Arl3-effector-GAP complex. *FEBS Lett.* 582:2501–2507. doi:10.1016/j.febslet.2008.05.053

West, R.R., K.M. Tenbarge, and J.B. Olmsted. 1991. A model for microtubule-associated protein 4 structure. Domains defined by comparisons of human, mouse, and bovine sequences. *J. Biol. Chem.* 266:21886–21896.

Williams, C.L., M.E. Winkelbauer, J.C. Schafer, E.J. Michaud, and B.K. Yoder. 2008. Functional redundancy of the B9 proteins and nephrocystins in *Caenorhabditis elegans* ciliogenesis. *Mol. Biol. Cell.* 19:2154–2168. doi:10.1091/mbc.E07-10-1070

Zhang, X., Z. Yuan, Y. Zhang, S. Yong, A. Salas-Burgos, J. Koomen, N. Olashaw, J.T. Parsons, X.J. Yang, S.R. Dent, et al. 2007. HDAC6 modulates cell motility by altering the acetylation level of cortactin. *Mol. Cell.* 27:197–213. doi:10.1016/j.molcel.2007.05.033

Zhou, C., L. Cunningham, A.I. Marcus, Y. Li, and R.A. Kahn. 2006a. Arl2 and Arl3 regulate different microtubule-dependent processes. *Mol. Biol. Cell.* 17:2476–2487. doi:10.1091/mbc.E05-10-0929

Zhou, F., Y. Xue, X. Yao, and Y. Xu. 2006b. CSS-Palm: palmitoylation site prediction with a clustering and scoring strategy (CSS). *Bioinformatics.* 22:894–896. doi:10.1093/bioinformatics/btl013